Monthly Notices
of the
ROYAL ASTRONOMICAL SOCIETY

Mon. Not. R. Astron. Soc. **423,** 1215–1220 (2012) doi:10.1111/j.1365-2966.2012.20948.x

A deep X-ray observation of the supernova remnant G304.6+0.1 (Kes 17) using *Suzaku*

F. Gök[1]★ and A. Sezer[2,3]★

[1]*Akdeniz University, Faculty of Education, Antalya 07058, Turkey*
[2]*TÜBİTAK Space Technologies Research Institute, ODTU Campus, Ankara 06531, Turkey*
[3]*Bogãzi çi University, Faculty of Art and Sciences, Department of Physics, Istanbul 34342, Turkey*

Accepted 2012 March 16. Received 2012 March 12; in original form 2011 December 13

ABSTRACT

In this paper, we present the analysis of a deep (99.6 ks) observation of G304.6+0.1 with the X-ray Imaging Spectrometer on board the *Suzaku* satellite. The X-ray spectral data are well fitted with a plasma model consisting of a thermal component, in collisional ionization equilibrium, and a non-thermal component. The thermal emission is well fitted with the VMEKAL model with an electron temperature of $kT_e \sim 0.75$ keV, a high absorbing column density of $N_H \sim 3.9 \times 10^{22}$ cm^{-2} and near/lower solar abundances, which indicate that the X-ray emitting plasma of G304.6+0.1 is dominated by a swept-up ambient medium. The non-thermal component is well fitted with a power-law model with a photon index of $\Gamma \sim 1.4$. We have found a relatively high electron density $n_e \sim 2.3f^{-1/2}$ cm^{-3}, an age $t \sim 1.4 \times 10^4 f^{1/2}$ yr and an X-ray emitting mass $M_x \sim 380f^{1/2}$ M$_\odot$ at an adopted distance of $d = 10$ kpc. Using the morphological and spectral X-ray data, we confirm that the remnant is a new member of the mixed-morphology supernova remnants.

Key words: ISM: individual objects: G304.6+0.1 (Kes 17) – ISM: supernova remnants – X-rays: ISM.

1 INTRODUCTION

Recent supernova remnant (SNR) observations in the X-ray band have led to the discovery of a considerable number of SNRs belonging to a new morphological class, called mixed-morphology (MM) SNRs, which are centrally bright in the X-ray band and are characterized by a thermal spectrum with little or no limb brightening and a shell morphology in radio (Rho & Petre 1998). Their characteristics have been explained by two basic scenarios: evaporating clouds (Cowie & Mckee 1977; White & Long 1991) and thermal conduction models (Cox et al. 1999; Shelton et al. 1999; Shelton, Kuntz & Petre 2004). In addition to these basic scenarios, there are new scenarios that try to explain the mechanism taking place. However, MM SNRs are still not understood completely. Deep X-ray observations will help us to understand the mechanism taking place in these MM SNRs.

G304.6+0.1 (Kes 17), a new MM member (Combi et al. 2010), was first detected at 408 MHz and 5 GHz with the Parkes and Molonglo radio telescopes by Shaver & Goss (1970). Caswell et al. (1975) gave a lower limit of 9.7 kpc to the distance of the remnant by measuring the 21-cm absorption profiles with the Parkes hydrogen-line interferometer. From the radio observations, Milne et al. (1985) have suggested that its structure results from the shock front collision with its dense environment. Whiteoak & Green (1996) have shown that it has an irregular shell morphology with a small size. Frail et al. (1996) have detected 1720-MHz OH maser emission towards G304.6+0.1 by using the Parkes telescope. Using mid-infrared (mid-IR) data from the Spitzer space telescope at 3.6, 4.5, 5.8 and 8 μm, Reach et al. (2006) have shown that the remnant has a shell structure in IR and they detected a pair of thin filaments at about RA (2000) = $13^h05^m46\overset{s}{.}2$, Dec. (2000) = $-62^\circ38'33''$. They claim that most of the IR emission coming from the shell could be a result of shocked molecular material. Hewitt et al. (2009) have obtained sensitive low-resolution spectroscopy from 5 to 35 μm for this remnant with the Spitzer Infrared Spectrograph (IRS) and they found evidence of shocked molecular gas. The first detailed multiwavelength (radio, mid-IR and X-ray) study of G304.6+0.1 has been conducted by Combi et al. (2010). Using *XMM–Newton* data (26.8 ks), they have found that the X-ray emission is dominated by thermal radiation (PSHOCK) plus a small fraction of non-thermal radiation (power law) in the northern, central and southern regions. They found a high column density N_H in the range of (2.5–3.5) $\times$ 10^{22} cm^{-2}, $kT_e \sim 0.75$ keV and the plasma was in a non-equilibrium ionization state with $\tau \sim 2.1 \times 10^{12}$ cm^{-3} s. In addition, they calculated the electron density n_e to be ∼0.99, ∼0.89 and ∼2.26 cm^{-3} for the northern, central and southern regions, respectively. Their multiwavelength study has suggested that this remnant is a middle-aged

★E-mail: gok@akdeniz.edu.tr (FG); aytap.sezer@boun.edu.tr (AS)

© 2012 The Authors
Monthly Notices of the Royal Astronomical Society © 2012 RAS

Downloaded from https://academic.oup.com/mnras/article/423/2/1215/961262 by Akdeniz University user on 20 September 2021

SNR, and belongs to the class of MM SNRs. Using data obtained with the *AKARI* and *Spitzer* satellites, Lee et al. (2011) have shown that the IR emission is concentrated on the western and southern shells – the western shell is bright in the mid-IR and far-IR continuum and the near-IR H_2 line emission, whereas the southern shell is visible only in the mid-IR continuum emission. They have suggested that the far-IR continuum and the near-IR H_2 line emission emanating from the western shell is the result of an interaction with a nearby molecular cloud. Using data from the Large Area Telescope on board the *Fermi* Gamma-ray Space Telescope, Wu et al. (2011) have reported on the discovery of GeV emission at the position of this remnant. They observed the remnant in the 1–20 GeV range with a significance of $\sim 12\sigma$, and they have suggested that Kes 17 is a candidate acceleration site for cosmic rays. They have reported the detection of a number of gamma-ray sources in its vicinity.

The newest Japanese X-ray astronomy satellite, *Suzaku* (Mitsuda et al. 2007), which has a good energy resolution, high efficiency and low background level for diffuse sources, has observed G304.6+0.1 with a 99.6-ks exposure time. Our aim is to study this remnant using high-quality spectral data, because its morphology implies that it has a similarity with the recently proposed group of MM SNRs.

The rest of this paper is structured as follows. We describe the observation and data reduction in Section 2, and we report on the image and spectral analyses in Section 3. We discuss the results of the spectral analysis in Section 3.2. Finally, in Section 4, we investigate the X-ray characteristics of G304.6+0.1 from radial spectral variations and we compare the results with the two basic scenarios used to explain the MM SNRs.

2 OBSERVATION AND DATA REDUCTION

Suzaku observed G304.6+0.1 with the X-ray imaging spectrometer (XIS; Koyama et al. 2007) on 2010 September 3, for 99.6 ks (Obs. ID: 505074010). *Suzaku* has three working XIS CCDs; two of the cameras (XIS0 and XIS3) have front-illuminated (FI) CCDs, and the remaining camera (XIS1) has a back-illuminated (BI) CCD. Each CCD camera has a single CCD chip with an array of 1024 × 1024 pixels, and each covers an area of 17.8 × 17.8 arcmin^2. The XIS was operated with normal clocking mode, in 5 × 5 and 3 × 3 editing modes.

We used the HEADAS 6.5 software package for data reduction. The XIS data have been screened with XSELECT using the standard criterion (Koyama et al. 2007). The spectral analysis and model fitting have been performed with XSPEC v11.3 (Arnaud 1996). The redistribution matrix files (RMFs) of the XIS have been produced by the xisrmfgen and auxilliary response files (ARFs) using xissimarfgen (Ishisaki et al. 2007).

3 ANALYSIS

3.1 Image analysis

Fig. 1 shows the XIS0 image of G304.6+0.1 in the 0.3–10 keV full-energy band. The outermost ellipse represents the overall region (which we call region 1) in which the X-ray emission originates. Inside region 1, the emission looks to be concentrated in two parts, the inner ellipse (which we call region 2) and the inner circle (which we call region 3). The dashed circle and dashed square show the background region and the XIS field of view (FOV), respectively. Fig. 2 shows the XIS0 image in the 0.3–10 keV band, overlaid with the contours of the 843-MHz radio image from Whiteoak & Green (1996).

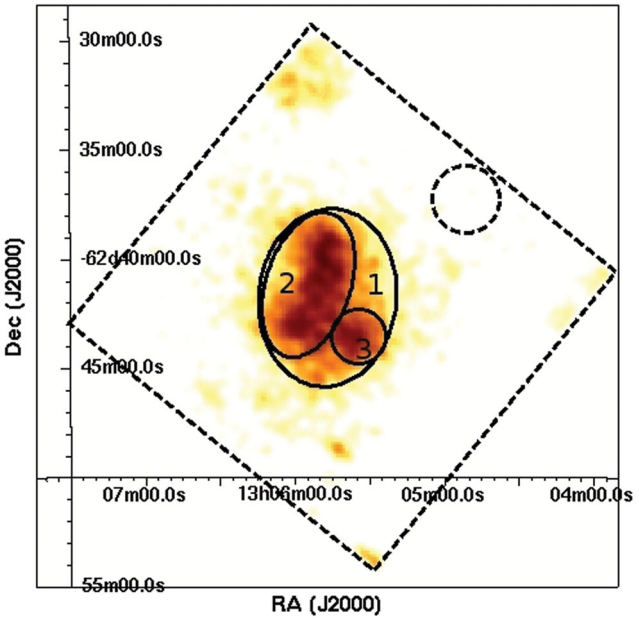


Figure 1. *Suzaku* XIS0 image of G304.6+0.1 in the 0.3–10 keV energy band. The outer and inner ellipses represent regions 1 and 2, respectively, and the inner circle represents region 3. The dashed circle and dashed square show the background region and the FOV of XIS0, respectively.

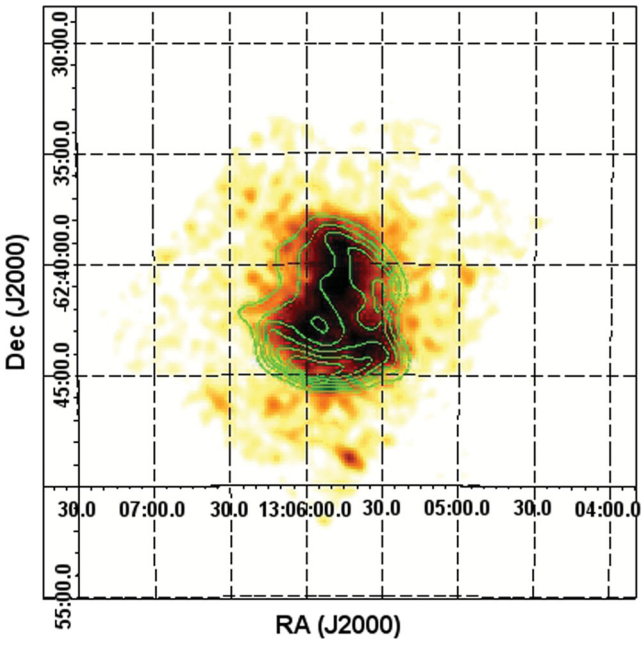


Figure 2. *Suzaku* XIS0 image of G304.6+0.1 in the 0.3–10 keV full-energy band, overlaid with contours of the 843-MHz radio image from Whiteoak & Green (1996). The X-ray image is smoothed with a Gaussian kernel of $\sigma = 2$ arcsec, and the units are in counts s^{-1}. Overlaid contours are spaced linearly in intensities of 0.07, 0.26, 0.44 and 0.62 count pixel^{-1}.

3.2 Spectral analysis

We extracted the spectrum for each XIS detector for the outer elliptical region, the inner elliptical region and the inner circular region. The background has been extracted from the circular region, taking care not to include the ^{55}Fe calibration sources in the corners of the CCD. Table 1 gives details of the ellipses, circles and background

Downloaded from https://academic.oup.com/mnras/article/423/2/1215/961262 by Akdeniz University user on 20 September 2021

Table 1. Centre coordinates, sizes and angles for regions 1, 2 and 3 and for the background.

Regions	Centre coordinates RA (2000), Dec. (2000) ($^{h\,m\,s}$, $^{\circ\,\prime\,\prime\prime}$)	Size (arcmin)	Angle (deg)
1	13 05 44, −62 41 54	3.2 × 4.1	354
2	13 05 55, −62 41 11	1.9 × 3.4	342
3	13 05 35, −62 43 33	1.24	0
Background	13 04 52, −62 37 16	1.56	0

(centre coordinates, sizes and angles). The spectra are grouped with a minimum of 50 counts bin^{-1} for region 1, 30 counts bin^{-1} for region 2 and 25 counts bin^{-1} for region 3, and χ^2 statistics is used.

For the spectral fitting of region 1, we first applied a single-temperature non-equilibrium ionization (NEI) model (VNEI in XSPEC; Borkowski, Lyerly & Reynolds 2001) modified by Galactic absorption via the WABS multiplicative model (Morrison & McCammon 1983). The parameters of the absorbing column density ($N_{\rm H}$), electron temperature ($kT_{\rm e}$) and ionization parameter ($\tau = n_{\rm e}t$) were set to be free parameters, while all elemental abundances were fixed at their solar values (Anders & Grevesse 1989). The model gave a large ionization parameter of $\tau \sim 10^{13}$ cm^{-3} s, which means that the plasma of the remnant has reached ionization equilibrium with a reduced χ^2 of 1.43 (948/664 d.o.f.). Therefore, we tried an absorbed collisional ionization equilibrium (CIE) plasma model (VMEKAL in XSPEC; Mewe, Gronenschild & van den Oord 1985; Mewe, Lemen & van den Oord 1986; Liedahl, Osterheld & Goldstein 1995). In this case, the reduced χ^2 value (926/665 = 1.39) improved slightly, but it was clear that the model fitting needed a second component. Therefore, we added a second thermal component to VMEKAL, a CIE model (VMEKAL) and a NEI model (VNEI), respectively. From the model fitting of VMEKAL+VMEKAL, we did not see two different temperatures, but when we thawed Mg, Si and S, we obtained two different temperatures of ∼0.6 and ∼1.1 keV, with a reasonably good reduced χ^2 of 1.15 (761.7/660 d.o.f.). However, we obtained an unphysically low abundance of S and very high errors for the abundances of Mg, Si and S. From the model fitting of VMEKAL+VNEI, we obtained two different temperatures of ∼0.6 and ∼1.4 keV. When we thawed Mg, Si and S, the χ^2 value improved significantly (750.8/659 = 1.14). For both model fittings we used the *F*-test to test whether the extra thermal component was a statistically significant addition. However, the *F*-test gave probabilities of $\sim 1.5 \times 10^{-7}$ and $\sim 6.9 \times 10^{-9}$ that the improvement is due to chance, for the VMEKAL+VMEKAL and VMEKAL+VNEI models, respectively. Then, we added a power-law component to the VMEKAL model. In this case, we obtained reasonably good physical parameter values and their errors with an acceptable χ^2 value (799/663 = 1.2). Then, we allowed Mg, Si and S to vary, which yielded a rather good reduced χ^2 value of 1.06 (700/660 d.o.f.). We also applied the *F*-test to our model fitting, which gave a probability of $\sim 1.2 \times 10^{-19}$ that the improvement is not due to chance. All these steps were repeated for regions 2 and 3. For region 2, the VMEKAL model required a power-law component. However, region 3 did not require a second component. The XIS0, XIS1 and XIS3 spectra of the three regions were fitted simultaneously in the 0.3–10 keV energy band and these are given in Figs 3(a), (b) and (c). The right panels of this figure show the individual components of the applied model, VMEKAL and power law, for XIS1 only. The best-fitting parameters of the applied models for the three regions are listed in Table 2. All the errors are at the 90 per cent confidence level.

We also studied spectral variation across the remnant and we give these results in Fig. 4. To study the radial variation of $kT_{\rm e}$ and surface brightness, we chose five elliptical annuli with 0.6 × 1.4, 1.3 × 2.1, 1.9 × 2.8, 2.7 × 3.6 and 3.6 × 4.7 arcmin^2 regions, centred at RA (2000) = $13^{\rm h}05^{\rm m}48^{\rm s}$, Dec. (2000) = $-62^\circ 41' 46''$ from the XIS0 FOV. The spectra extracted from the elliptical annuli were grouped with a minimum of 20 counts bin^{-1}. We applied our best-fitting model (an absorbed VMEKAL and power law) starting from the central region within 0.6 × 1.4 arcmin^2, and we allowed the absorbing column density, electron temperature, normalization and abundances of Mg, Si and S to vary. For all outer annuli, we applied the same model fixing $N_{\rm H}$ to the value obtained from the central region.

4 DISCUSSION AND CONCLUSIONS

In this work, we have studied the X-ray morphology and spectral properties of G304.6+0.1 using XIS data obtained with a deep

Table 2. Best-fitting parameters with corresponding errors at the 90 per cent confidence level in the 0.3–10 keV energy band.

Component	Parameters	Region 1	Region 2	Region 3
WABS	$N_{\rm H}$(× 10^{22} cm^{-2})	3.9 ± 0.1	4.2 ± 0.1	3.2 ± 0.1
VMEKAL	$kT_{\rm e}$(keV)	0.75 ± 0.01	0.74 ± 0.01	0.84 ± 0.03
Abundance[a]	Mg	1.3 ± 0.2	1.2 ± 0.2	0.9 ± 0.2
	Si	0.9 ± 0.1	0.9 ± 0.1	1.1 ± 0.1
	S	0.6 ± 0.1	0.5 ± 0.1	0.4 ± 0.1
	Norm (photons cm^{-2}s^{-1})	0.93 ± 0.06	0.65 ± 0.11	0.07 ± 0.01
	EM[b]	11.1 ± 0.8	7.7 ± 1.1	0.8 ± 0.1
	Flux[c]	4.6 ± 0.1	3.2 ± 0.2	0.6 ± 0.1
Power law	Photon index	1.4 ± 0.1	1.6 ± 0.2	–
	Norm (× 10^{-2} photons cm^{-2} s^{-1})	1.17 ± 0.23	0.46 ± 0.21	–
	Flux[d]	5.5 ± 0.2	3.6 ± 0.2	–
	χ^2/d.o.f.	700/660=1.06	747/657=1.14	253.8/192=1.32

[a] Abundances are relative to the solar values (Anders & Grevesse 1989).
[b] Emission measure $EM = \int n_{\rm e} n_{\rm H}\, {\rm d}V$ in units of 10^{59} cm^{-3}, where $n_{\rm e}$ and $n_{\rm H}$ are the number densities of electrons and protons, respectively and V is the X-ray emitting volume.
[c] Absorption-corrected thermal flux in the 0.3–10 keV energy band in units of 10^{-11} erg s^{-1} cm^{-2}.
[d] Absorption-corrected total flux (VMEKAL plus power-law components) in the 0.3–10 keV energy band in units of 10^{-11} erg s^{-1} cm^{-2}.

Downloaded from https://academic.oup.com/mnras/article/423/2/1215/961262 by Akdeniz University user on 20 September 2021

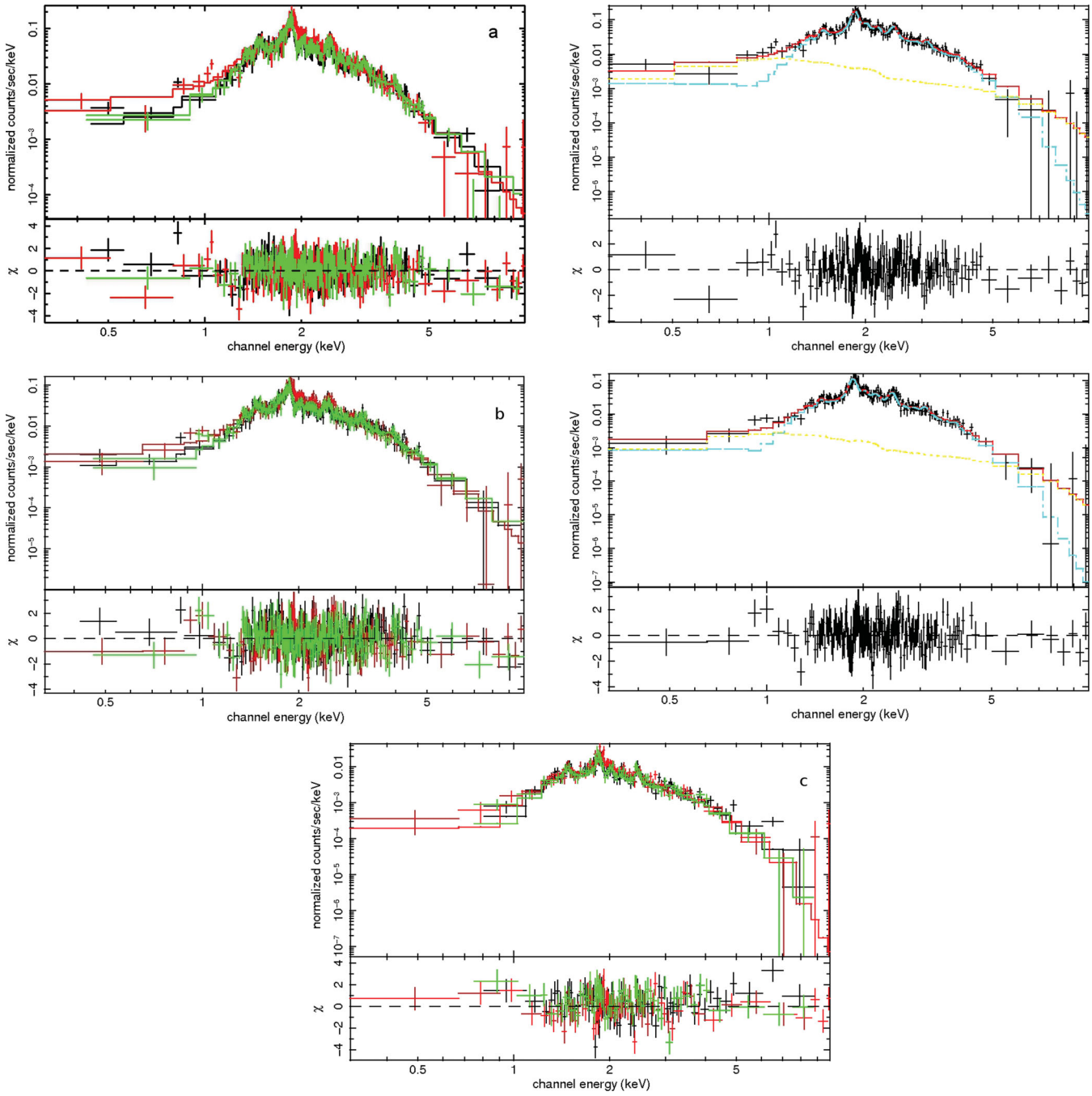


Figure 3. Upper-left panels: *Suzaku* XIS (XIS0, black; XIS1, red; XIS3, green) spectra have been fitted by an absorbed VMEKAL+power-law model in the 0.3–10 keV energy band simultaneously: (a) region 1; (b) region 2. Upper-right panels: the red curve represents the best fit of the two-component model (VMEKAL+power-law). The individual components are represented by the cyan curve for the VMEKAL model and the yellow curve for the power-law model only for XIS1 for regions 1 and 2. Bottom panel (c): the XIS spectra have been fitted by an absorbed VMEKAL model in the 0.3–10 keV energy band simultaneously for region 3. The lower panels show the residual in units of σ.

observation by *Suzaku*. As seen from Fig. 2, G304.6+0.1 has a centrally filled X-ray morphology dominated by thermal X-ray emission, and the radio contours of this remnant are concentrated at its shell. Morphologically, this remnant resembles the MM SNRs. With the help of high-quality spectral data, we have studied the spectral characteristics of G304.6+0.1 and here we compare our findings with the theoretical models proposed for MM SNRs.

The X-ray emission from the remnant is well described by the model of a thermal plasma that has reached ionization equilibrium. The non-thermal component (power law) required to describe the plasma state has a photon index (Γ) of $\sim$1.4. The dominant emission from this remnant is thermal ($\sim$90 per cent of the total X-ray flux) and it is described by the CIE plasma model (in CIE plasma, $n_e t$ should be larger than 10^{12} cm^{-3} s; Masai 1984) with an electron temperature of $kT_e \sim 0.75$ keV. We have performed detailed spectral fitting for three regions. As seen from Table 2, the spectral parameters for the three regions are almost similar. We obtained a high absorbing column density N_H in the range of (3.2–4.2) $\times$

Downloaded from https://academic.oup.com/mnras/article/423/2/1215/961262 by Akdeniz University user on 20 September 2021

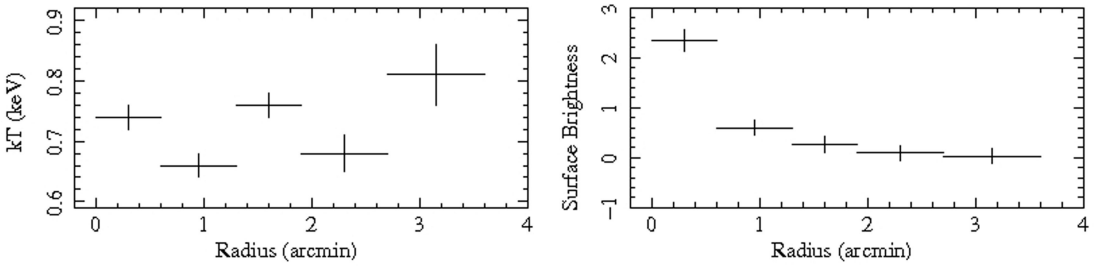


Figure 4. The radial profiles of electron temperature (left panel) and surface brightness (right panel) obtained from the XIS0 spectra. The surface brightness is in units of $\times\ 10^{-12}$ erg s^{-1} cm^{-2} arcmin^{-2} in the 0.3–10 keV energy band.

10^{22} cm^{-2}, which is consistent with the previous work of Combi et al. (2010), in the range of (2.5–3.5) $\times\ 10^{22}$ cm^{-2}. This gives support for the large distance $d \geq 9.7$ kpc to the remnant adopted by Caswell et al. (1975). Our $N_{\rm H}$ value is larger than that of Combi et al. (2010) and therefore, throughout our calculations, we have used $d =$ 10 kpc. From the emission measure ($EM = n_{\rm e} n_{\rm H} V$, where $n_{\rm e}$ is the electron density, $n_{\rm H}$ is the hydrogen density and V is the volume of the X-ray emitting plasma), we estimate the electron density of the plasma, taking into account $n_{\rm e} = 1.2 n_{\rm H}$ for the mean charge state with normal composition. Considering the possibility that less than the entire volume is filled, we calculate the volume of the X-ray emitting region from $V = (4/3)\pi R^3 f$, where R is the SNR radius and f is the filling factor. Then, we carry the f factor through our calculations to see the dependence of each derived quantity (e.g. electron density, age) on f. We find that the volume is $\sim 1.9 \times 10^{59} f$ cm^3, assuming a spherical radius of 4 arcmin at the distance $d = 10$ kpc, and then the electron density is $\sim 2.3 f^{-1/2}$ cm^{-3}. When calculating the age of the remnant, we use the relation $\tau / n_{\rm e}$, where τ is the ionization age of the plasma. The CIE model gives only a lower limit (10^{12} cm^{-3} s) to this parameter, and hence it leads to a lower limit on the age t of the remnant, which is calculated to be $\sim 1.4 \times 10^4 f^{1/2}$ yr for G304.6+0.1. The mass of the X-ray emitting gas is calculated to be $\sim 380 f^{1/2}$ M$_\odot$ from $M_{\rm x} = m_{\rm H} n_{\rm e} V$, where $m_{\rm H}$ is the mass of a hydrogen atom. As seen from Table 2, the near/lower solar abundance values obtained for each region and the large X-ray emitting mass indicate that the X-ray emission results from the swept-up ambient medium, as is generally the case for middle-aged SNRs. The relatively large $n_{\rm e}$ ($\sim 2.3 f^{-1/2}$ cm^{-3}) and small size ($\sim$8 arcmin) suggest that the remnant expands in a region with a large ambient density.

For the non-thermal component that constitutes $\sim$10 per cent of the total flux, our best-fitting photon index is in the range of 1.4–1.6, as seen in Table 2. This is consistent with that of classical young pulsars ranging between 1.1 and 1.7 (Chakrabarty et al. 2001). However, there is no compact or extended X-ray source reported at the location of or in the vicinity of this remnant. Another possibility could be that the power-law emission results from the synchrotron emission from shock-accelerated relativistic electrons. Also, the *Fermi* detection of G304.6+0.1 (Wu et al. 2011) appears to be related to the remnant and not to a central compact object. However, our spectral fitting of each elliptical annulus gives a different photon index value ($\Gamma \sim 1.5$, 1.2, 1.3 and 1.5). Moreover, the photon index obtained from the centre is unphysically large ($\Gamma \sim 7.3$), which indicates that the power-law emission cannot be related to the remnant itself. The fact that our best-fitting model required no non-thermal component for region 3 might support this idea. Considering all these cases, it is still difficult to explain the origin of the non-thermal emission using *Suzaku* data. Combi et al. (2010) also obtained non-thermal emission from this remnant with a photon index value in the range of 1.8–3.1 with an *XMM–Newton* observation, which is softer than our photon index value. This indicates particle acceleration in shock fronts.

In addition to morphological evidence, G304.6+0.1 is a middle-aged ($\sim 10^4$ yr) SNR, the plasma of the remnant is in a CIE condition and it is located in an inhomogeneous medium. The general characteristics of MM SNRs have been given in Rho & Petre (1998) as follows. (i) Members of this class have a centrally peaked morphology in the X-ray band, characterized by a thermal spectrum while having a shell morphology in radio. (ii) Their ages are expected to be $\sim 10^4$ yr, which means that the plasma should be in a CIE condition. (iii) They are interacting with molecular clouds and/or H I clouds, which means that they are located in a very dense medium. Considering these properties, we can say that G304.6+0.1 is likely to be a member of the class of MM SNRs, as suggested by Combi et al. (2010). The two basic scenarios explaining this class are as follows. (i) The interior X-ray emission arises from the gas evaporated from shocked clouds (Cowie & Mckee 1977; White & Long 1991). (ii) As an SNR evolves, the temperature and density of the hot interior plasma gradually become uniform through thermal conduction, the temperature in the outer shells becomes lower and is absorbed by the interstellar medium, and the only detectable X-ray emission emanates from the interior of the SNR (Cox et al. 1999; Shelton et al. 1999, 2004). To compare our results with these models, we have studied the radial variations of $kT_{\rm e}$ and the surface brightness, as seen from Fig. 4. We have found that the temperature variation ($kT_{\rm e} \sim$ 0.66–0.81 keV) is almost uniform across the remnant, as predicted by both models. In contrast, the surface brightness peaks at the centre and declines towards the shell regions from $\sim 2.34 \times 10^{-12}$ to $\sim 0.03 \times 10^{-12}$ erg s^{-1} cm^{-2} arcmin^{-2} in 0.3–10 keV, which is consistent with the model of evaporating clouds. G304.6+0.1 is interacting with an OH maser source at 1720 MHz (Frail et al. 1996). Recently, Lee et al. (2011) have suggested that the remnant is interacting with a nearby molecular cloud. Furthermore, Wu et al. (2011) have detected GeV emission from the SNR and a number of gamma-ray sources in its vicinity. The thermal conduction model requires a relatively high density ambient medium, while the evaporation model requires dense clouds. In this respect, G304.6+0.1 is consistent with both models.

Here, we present the results from the *Suzaku* archival data of G304.6+0.1. The deep XIS spectra consist of two components; the thermal emission coming from the plasma is in a CIE condition with $kT_{\rm e} \sim 0.75$ keV and a high $N_{\rm H}$ value, and the non-thermal emission has a photon index of $\sim$1.4. This value is consistent with that of classical young pulsars, but there has been no observed compact source reported. So, the origin of the non-thermal emission is still unclear. The thermal emission originates from the shocked

Downloaded from https://academic.oup.com/mnras/article/423/2/1215/961262 by Akdeniz University user on 20 September 2021

ambient medium with an electron density of $n_e \sim 2.3f^{-1/2}$ cm^{-3}. The morphological and X-ray spectral characteristics imply that G304.6+0.1 is a member of the MM class of SNRs.

ACKNOWLEDGMENTS

We thank the referee for detailed and constructive comments and suggestions on the manuscript. We also acknowledge support from the Akdeniz University Scientific Research Project Management. AS is supported by a TÜBİTAK Postdoctoral Fellowship.

REFERENCES

Anders E., Grevesse N., 1989, Geochim. Cosmochim. Acta, 53, 197
Arnaud K. A., 1996, in Jacoby G., Barnes J., eds, ASP Conf. Ser. Vol. 101, Astronomical Data Analysis Software and Systems V. Astron. Soc. Pac., San Francisco, p. 17
Borkowski K. J., Lyerly W. J., Reynolds S. P., 2001, ApJ, 548, 820
Caswell J. L., Murray J. D., Roger R. S., Cole D. J., Cooke D. J., 1975, A&A, 45, 239
Chakrabarty D., Pivovaroff M. J., Hernquist L. E., Heyl J. S., Narayan R., 2001, ApJ, 548, 800
Combi J. A. et al., 2010, A&A, 523, 76
Cowie L. L., McKee C. F., 1977, ApJ, 211, 135
Cox D. P., Shelton R. L., Maciejewski W., Smith R. K., Plewa T., Pawl A., Róýyczka M., 1999, ApJ, 524, 179
Frail D. A., Goss W. M., Reynoso E. M., Giacani E. B., Green A. J., Otrupcek R., 1996, AJ, 111, 1651
Hewitt J. W., Rho J., Andersen M., Reach W. T., 2009, ApJ, 694, 1266
Ishisaki Y. et al., 2007, PASJ, 59, 113
Koyama K. et al., 2007, PASJ, 59, 23
Lee H. G., Moon D. S., Koo B. C., Onaka T., Jeong W. S., Shinn J. H., Sakon I., 2011, ApJ, 740, 31
Liedahl D. A., Osterheld A. L., Goldstein W. H., 1995, ApJ, 438, L115
Masai K., 1984, Ap&SS, 98, 367
Mewe R., Gronenschild E. H. B. M., van den Oord G. H. J., 1985, A&AS, 62, 197
Mewe R., Lemen J. R., van den Oord G. H. J., 1986, A&AS, 65, 511
Milne D. K., Caswell J. L., Haynes R. F., Kesteven M. J., Wellington K. J., Roger R. S., Bunton J. D., 1985, PASA, 6, 78
Mitsuda K. et al., 2007, PASJ, 59, 1
Morrison R., McCammon D., 1983, ApJ, 270, 119
Reach W. T. et al., 2006, AJ, 131, 1479
Rho J., Petre R., 1998, ApJ, 503, L167
Shaver P. A., Goss W. M., 1970, Australian J. Phys. Astrophys. Suppl., 17, 133
Shelton R. L., Cox D. P., Maciejewski W., Smith R. K., Plewa T., Pawl A., Róýyczka M., 1999, ApJ, 524, 192
Shelton R. L., Kuntz K. D., Petre R., 2004, ApJ, 611, 906
White R. L., Long K. S., 1991, ApJ, 373, 543
Whiteoak J. B. Z., Green A. J., 1996, A&AS, 118, 329
Wu J. H. K., Wu E. M. H., Hui C. Y., Tam P. H. T., Huang R. H. H., Kong A. K. H., Cheng K. S., 2011, ApJ, 740, L12

This paper has been typeset from a TEX/LATEX file prepared by the author.

Downloaded from https://academic.oup.com/mnras/article/423/2/1215/961262 by Akdeniz University user on 20 September 2021